Polymer 340 (2025) 129241

Contents lists available at ScienceDirect

Polymer

journal homepage: www.elsevier.com/locate/polymer

Enhanced toughness and thermal stability of OVPOSS-copolymerized isophthalic unsaturated polyester resin: A microstructural mechanism study

Chunlong Li, Mengdan Di, Huige Wei, Kangfu Sun *, Jingguo Cao **

College of Chemical Engineering and Material Science, Tianjin University of Science & Technology, Tianjin, 300457, China

ARTICLE INFO

Keywords:
Unsaturated polyester resin
POSS
Molecular dynamics simulation
Glass transition temperature

ABSTRACT

Unsaturated polyester resin (UPR) is widely utilized in modern automotive and construction industries due to its versatility, superior mechanical properties, and ease of processing. However, traditional toughening strategies often compromise its thermal stability, significantly limiting its practical applications. In this study, octavinyl cage-type polyhedral oligomeric silsesquioxane (OVPOSS) was synthesized via silane hydrolysis-condensation and subsequently copolymerized with UPR to prepare a novel UPR/VIPS resin (VIPS: vinyl-functionalized POSS). The structural characterization of the resulting resin was performed using NMR, FTIR, and XPS techniques, and its microstructural properties were further investigated through molecular dynamics (MD) simulations. The incorporation of OVPOSS significantly enhanced both the mechanical strength and thermal stability of UPR, with the flexural strength and heat distortion temperature (HDT) increasing by 48.2 % and 24.0 °C, respectively, compared to neat UPR. MD simulations demonstrated that the vinyl groups on the periphery of OVPOSS copolymerized with UPR chains, forming an interpenetrating polymer network (IPN) that synergistically interacted with the rigid inorganic siloxane cage core. This synergy effectively restricted polymer chain mobility and thermal conductivity, thereby enhancing the overall structural integrity and thermal resistance of the resin, consistent with the experimental findings. These results suggest that the POSS-based UPR/VIPS modification strategy provides a promising approach for the development of unsaturated polyester resins with enhanced mechanical performance, thermal stability, and a well-balanced set of properties.

1. Introduction

In recent years, polymers and their composites have garnered significant attention in the fields of materials science and engineering, and have found widespread applications in industries such as aerospace, automotive, electronics, oil and gas, and construction. Among these materials, unsaturated polyester resin (UPR) is extensively used as a matrix for high-performance fiber-reinforced composites, owing to its stable physicochemical properties, ease of processing, and strong interfacial adhesion with most reinforcing fibers. Additionally, UPR is a widely utilized commercial thermosetting resin for various applications, including insulating materials, coatings, and structural components [1–3]. Despite its advantages, UPR suffers from several inherent drawbacks, including poor thermal stability, low toughness, and high brittleness, which limit its further use in advanced composites—such as carbon fiber-reinforced systems. Of particular concern is the thermal stability of UPR, which significantly affects the dimensional stability and service performance of composite materials. Consequently, improving both the mechanical properties and thermal stability of UPR to enhance its performance at elevated temperatures and improve its structural reliability has become a major research focus worldwide [4].

At present, the primary modification strategies for UPR include: (1) physical blending with a secondary phase, such as liquid rubber, nanoparticles, or thermoplastics [5–7]; (2) chemical modification through crosslinking reactions or copolymerization with monomers [8, 9]; and (3) the construction of interpenetrating polymer network (IPN) to enhance the overall mechanical properties and thermal stability via physical entanglement [10,11]. However, improving a specific property often results in undesirable trade-offs in others. For instance, the incorporation of liquid rubber at a loading of 15–20 phr leads to a

* Corresponding author. No.9, Thirteenth Street, Binhai New Area Economic and Technological Development Zone, Tianjin University of Science & Technology, Tianjin, 300457, China.
** Corresponding author. No.9, Thirteenth Street, Binhai New Area Economic and Technological Development Zone, Tianjin University of Science & Technology, Tianjin, 300457, China.
E-mail addresses: skf@tust.edu.cn (K. Sun), cjg@tust.edu.cn (J. Cao).

https://doi.org/10.1016/j.polymer.2025.129241
Received 28 July 2025; Received in revised form 4 October 2025; Accepted 21 October 2025
Available online 22 October 2025

decrease in the glass transition temperature (T_g), Young's modulus, and strength of the resin matrix [12]. Unmodified nanoparticles tend to agglomerate due to their high surface energy, which results in stress concentration, deterioration of mechanical properties, and a significant increase in viscosity. Chemical modification can enhance the crosslinking density of resins; however, it frequently results in a reduction of the T_g due to the incorporation of flexible chain segments and the dilution of crosslinking agents [13–15].

Recently, inorganic–organic nanohybrid materials have experienced rapid development as a new class of advanced materials. Polyhedral oligomeric silsesquioxanes (POSS), a representative type of nanohybrid material with a cage-like structure, exhibit both the high thermal stability and excellent mechanical properties of inorganic materials, as well as the high toughness and processability typical of organic materials [16]. POSS, the smallest, monodisperse silica cube-type nanoparticle of molecular silica, 1–1.5 nm in size, has the chemical formula $(RSiO_{1.5})_n$, where R for this study is an organic vinyl group attached to the corners of the cube. POSS molecule has a precisely defined structure with a rigid, cubic inorganic silica cage core with 0.53 nm side lengths and eight easily functionalized groups located on the corners of the cube [17]. In the preparation of nanocomposites, the key advantage of POSS lies in the diversity of its modifiable functional groups in combination with its three-dimensional structure. The siloxane core not only provides rigidity, but also imparts thermal and mechanical properties comparable to those of conventional ceramic materials. Meanwhile, the organic substituents enable functional modification, serving as compatibilizers to improve processability or as linkers to chemically bond with the organic matrix. These unique features make POSS one of the most promising candidates for polymer modification [18–20].

It is worth noting that POSS, with its inorganic siloxane cage core and organic peripheral groups, has the potential to integrate the advantages of both components, thereby achieving a balanced enhancement of multiple material properties [21]. Numerous studies have explored the incorporation of POSS to improve various properties of polymer resins. For example, Liu successfully synthesized a novel nano-flame retardant (PoDOH) using octabenzyl-POSS (OPS) as a precursor, which increased the limiting oxygen index (LOI) of epoxy resin (EP) from 25.1 % to 33.6 % and enhanced the Young's modulus by 25.35 % [22]. Zhang reported that the addition of POSS resulted in a 40 % improvement in the fracture toughness of the resin at 77 K [23]. Yang modified POSS via an efficient thiol–ene click reaction to introduce EMP groups, which improved the compatibility and reactivity of POSS with the resin matrix [24]. Xu investigated the influence of different organic substituents and POSS loadings on the thermal stability of silicone resins by incorporating various functionalized POSS molecules [16].

Despite significant progress in resin modification using POSS, several challenges remain unresolved. On the one hand, excessive incorporation of POSS into the resin may lead to agglomeration, which causes uneven stress distribution within the material and eventually results in damage [25,26]. Previous studies have shown that POSS with unsaturated substituents can undergo copolymerization with polymer chains, significantly enhancing the mobility of polymer chains and improving mechanical properties while mitigating the agglomeration effect to some extent. On the other hand, the synthesis of the target POSS building blocks involves multiple complex steps, and the POSS cages within hybrid materials are prone to breakage during subsequent processing. Consequently, selecting appropriate substrates for modified POSS, and determining its role in blending and copolymerization, has become a critical issue [27,28]. Given the unique characteristics and advantages of POSS and UPR, this research direction offers a promising avenue for material researchers seeking to develop practical applications.

With the continuous advancement of molecular simulation techniques, MD has been increasingly applied to the study of POSS-containing resin systems [29,30]. Blanco investigated the thermal stability of novel bridged POSS/polystyrene (PS) nanocomposites via MD simulations and reported notable improvements, highlighting the critical role of POSS/PS interactions at the polymer–filler interface [31]. Li systematically characterized the epoxy resin EPON862 and the curing agent DETDA using MD simulations, revealing the correlations among glass transition temperature (T_g), Young's modulus, and yield stress with respect to polymerization degree [32]. Kim employed molecular dynamics (MD) simulations to investigate the interfacial properties between fillers and the resin matrix, establishing the relationship between the interfacial behavior of nano-silica composites and the resin crosslinking density, and further calculating the thermal expansion coefficient and elastic modulus through simulations [33]. Nevertheless, studies on unsaturated polyester resin (UPR) with simultaneously enhanced mechanical and thermal properties remain relatively scarce. The incorporation of POSS, with its unique inorganic–organic hybrid cage structure, into UPR matrices offers a promising strategy to overcome the performance trade-offs typically observed in conventional UPR systems. This approach is expected to improve the comprehensive properties of UPR and expand its application potential in high-performance materials [34].

In this study, a high-toughness, high-thermal stability UPR modified with POSS was designed. Specifically, an isophthalic unsaturated polyester resin was selected as the primary toughening matrix component. A simple and effective OVPOSS was synthesized via silane hydrolysis-condensation to achieve good reactivity with UPR, thereby preventing phase separation. A one-pot method was used to prepare a homogeneous POSS-modified UPR/VIPS resin. The structures of OVPOSS and the modified composite materials were characterized using NMR, FTIR, XPS, and other analytical techniques. In parallel, MD simulations were employed to investigate the microscopic modification mechanism of POSS in UPR, analyzing its effects on the mechanical properties and thermal stability of UPR and providing a thorough discussion of the underlying mechanism. The results indicate that the introduction of OVPOSS leads to the formation of chemical bonds and physical entanglements between the vinyl organic functional groups on the periphery of OVPOSS and the isophthalic unsaturated polyester resin matrix. This reduces the free volume while increasing the crosslinking density, disperses stress, and slows the heat transfer at chain ends. Consequently, the balance between thermal stability and mechanical properties is maintained, with experimental and simulation results showing that the mechanical properties and thermal stability of the UPR/VIPS resin system are significantly improved to varying degrees.

2. Experiment

2.1. Materials

The isophthalic unsaturated polyester resin containing 35 wt% styrene was supplied by Tianjin Xinyang Technology Co., Ltd. (Tianjin, China). Vinyltrimethoxysilane (VTMS, 98 %), dichloromethane (DCM, 99 %), tetrahydrofuran (THF, 99 %), cobalt 2-ethylhexanoate (65 wt% in mineral spirits), methyl ethyl ketone peroxide (MEKP, >52 %), and hydroquinone (99 %) were purchased from Macklin Biochemical Technology Co., Ltd. (Shanghai, China). Acetone (≥99.9 %) was obtained from Fuchen (Tianjin) Chemical Reagent Co., Ltd. (Tianjin, China). Hydrochloric acid (HCl, 37 %) and the defoamer (VATIX-1050) were provided by Beijing Sino Composite Co., Ltd. (Beijing, China), while the release agent (1367 EZ) was supplied by Kentian (Shanghai) Trading Co., Ltd. (Shanghai, China). All reagents and solvents were of analytical grade and were used as received without further purification.

2.2. Preparation of UPR/VIPS resin systems

The resin system without OVPOSS was designated as Pure UPR, while the formulations containing OVPOSS were labeled according to the OVPOSS loading: 0.67 wt% (UPR/VIP-1), 0.83 wt% (UPR/VIP-2), 1.00 wt% (UPR/VIP-3), 1.17 wt% (UPR/VIP-4), and 1.33 wt% (UPR/

VIP-5).

As illustrated in Fig. 1a, the UPR/VIPS resin systems were synthesized via a straightforward one-pot method. Specifically, 600 g of isophthalic UPR was added to a beaker. In parallel, 4 g (0.67 wt%), 5 g (0.83 wt%), 6 g (1.00 wt%), 7 g (1.17 wt%), and 8 g (1.33 wt%) of OVPOSS were each dissolved in 20 mL of tetrahydrofuran (THF) to obtain transparent solutions. These OVPOSS/THF solutions were then gradually added to the polyester resin under vigorous stirring, followed by high-speed homogenization for 30 min to ensure uniform dispersion. Subsequently, 0.5 mL of hydroquinone solution (5 wt% in ethanol) and 0.5 mL of defoaming agent (VATIX-1050) were introduced into the mixture under continuous stirring. After complete blending, 9 g (1.5 wt

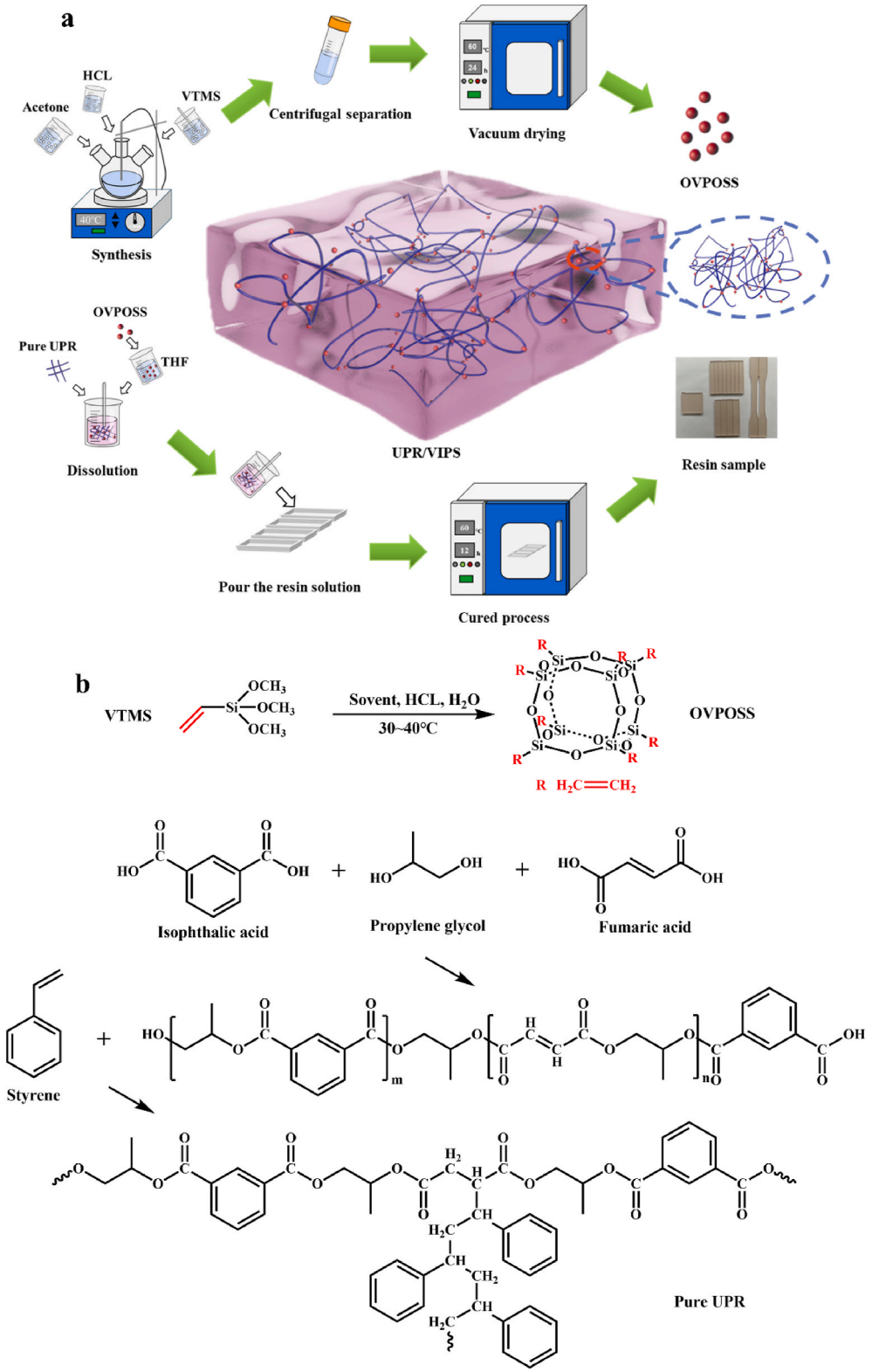

Fig. 1. a) Schematic illustration of the preparation process of OVPOSS and the UPR/VIPS resin system; b) Synthetic route of OVPOSS and the Pure UPR resin system.

%) of methyl ethyl ketone peroxide (MEKP) was added as the curing initiator, and the system was stirred for an additional 1 min. The resulting mixture was then degassed under vacuum until no visible bubbles remained. The prepared resin was cast into molds pre-coated with a release agent and cured at 25 ± 2 °C for 24 h, followed by post-curing at 60 °C for 12 h to ensure complete crosslinking.

The Pure UPR sample was prepared using the same procedure, except that no OVPOSS was incorporated.

2.3. Characterization and testing

2.3.1. Morphology and structural characterization

The molecular structures of OVPOSS and the UPR/VIPS resin systems were characterized by nuclear magnetic resonance (NMR) spectroscopy using a Bruker Avance NEO spectrometer (Bruker, Germany). Both ^{1}H NMR (operating frequency 400.15 MHz) and ^{29}Si NMR (operating frequency 79.49 MHz) spectra were recorded in deuterated chloroform ($CDCl_3$). Fourier-transform infrared spectroscopy (FTIR, TENSOR27) was employed to analyze the chemical structures and functional groups of OVPOSS and UPR/VIPS resins over the wavenumber range of 500–4000 cm^{-1}.

X-ray photoelectron spectroscopy (XPS, K-Alpha, Thermo Scientific) was conducted to investigate the elemental composition and chemical bonding states of OVPOSS and the resin matrices. The microstructure and surface morphology of the cured UPR/VIPS resins were observed using a field-emission scanning electron microscope (FE-SEM, SU8600, Hitachi, Japan).

2.3.2. Thermal stability and dielectric property testing

Differential scanning calorimetry (DSC, DSC204 F1, NETZSCH, Germany) was performed under a continuous nitrogen atmosphere (50 mL/min) with a heating rate of 10 °C/min from 25 °C to 250 °C. The sample mass was approximately 10 ± 0.1 mg, sealed in aluminum crucibles. The glass transition temperature (T_g) was determined as the midpoint of the heat capacity change. The thermal stability of the resin systems was evaluated using a simultaneous thermal analyzer (SDT-Q600, TA Instruments, USA) under a continuous nitrogen flow of 50 mL/min. The samples were heated from 25 °C to 800 °C at a constant rate of 10 °C/min. The thermal degradation temperature ($T_{d5\ \%}$) was defined as the temperature corresponding to a 5 % weight loss of the resin. The heat deflection temperature (HDT) was measured using a Vicat softening point tester (ZWK1302-S, MTS Systems (China) Co., Ltd.). The test was conducted in methyl silicone oil at a heating rate of 120 °C/h. Rectangular resin specimens with dimensions of 80 mm × 10 mm × 4 mm were used for HDT measurements. The dielectric constant was measured using a dielectric constant tester (ZJD-C, Zhonghang Times (China) Co., Ltd.) at 25 ± 2 °C in the frequency range of 0.1–50 MHz, employing copper parallel-plate electrodes. The resin samples were circular with a diameter of 50 mm and a thickness of 4 mm. Prior to testing, the samples were dried under vacuum at 60 °C for 5 h.

2.3.3. Mechanical properties testing

The tensile and flexural properties of the resin samples were evaluated using a microcomputer-controlled universal testing machine (CMT4304, MTS Systems (China) Co., Ltd.) in accordance with the GB/T 2567-2008 standard. Tensile tests were conducted at a crosshead speed of 2 mm/min with a gauge length of 50 mm, using dumbbell-shaped specimens measuring 200 mm × 10 mm × 4 mm. Flexural tests were performed at the same loading rate with a span length of 60 mm, using rectangular specimens measuring 90 mm × 15 mm × 4 mm.

The unnotched impact strength was determined using a pendulum impact tester (ZBC850, MTS Systems (China) Co., Ltd.) according to the GB/T 1043.1 standard. Test specimens had dimensions of 80 mm × 10 mm × 4 mm and a span length of 60 mm. The impact strength was calculated using Equation (1):

$$\sigma = \frac{1000A}{b \times h} \tag{1}$$

where A is the absorbed impact energy, b is the specimen width, and h is the specimen thickness. The impact strength was reported in kJ/m^2. For each formulation, at least four valid specimens were tested to ensure result reliability. Hardness measurements were carried out using a Barcol hardness tester on specimens measuring 50 mm × 50 mm × 4 mm. A minimum of ten hardness values was recorded for each sample.

2.4. Model construction and optimization

The initial crosslinked resin model was constructed using the Construction module in Amorphous Cell. The optimization was performed with the Smart algorithm, and the calculation effort was set to Medium. The COMPASS II force field was selected for the simulations. As depicted in Fig. S1 and Fig. 3a, geometrically optimized molecular structures of each component were randomly packed into a periodic simulation box, with an initial density of 0.95 g/cm^3 and a temperature of 300 K [35, 36]. Prior to performing MD simulations, energy minimization was carried out to eliminate steric hindrances and physically unreasonable configurations. Geometry optimization proceeded iteratively until convergence criteria were satisfied. Three key parameters—density, energy, and temperature—were monitored to determine whether the system had reached equilibrium. Specifically, density fluctuations were constrained within ±0.025 g/cm^3, energy variations were maintained below 5 %, and temperature fluctuations were kept within ±15 K. Upon meeting these conditions, the system was considered equilibrated.

To eliminate residual stress and improve structural relaxation, the system underwent an annealing process, which is essential for accurately simulating the crosslinked network of UPR. Each system was subjected to two NVT ensemble MD simulations at 300 K for 100 ps. The Andersen thermostat was used to control temperature, and pressure regulation was achieved via the Berendsen barostat. Following annealing, the lowest-energy conformation was extracted and heated under the NVT ensemble to 600 K, a temperature exceeding the glass transition temperature of the resin, to ensure sufficient chain mobility. Subsequently, NPT ensemble dynamics were performed at 0.0001 GPa for 100 ps to achieve structural equilibration and obtain reliable conformational configurations for further property analysis.

3. Results and discussion

3.1. Structural characterization

The synthesis procedure of OVPOSS is provided in the Supporting Information, and its synthetic route is illustrated in Fig. 1b. Using vinyltrimethoxysilane as the precursor, a cage-like molecular architecture was constructed via hydrolytic condensation under acidic conditions. OVPOSS, a representative organic–inorganic hybrid nanomaterial from the POSS family, features a rigid siloxane cage core surrounded by peripheral vinyl groups, forming a distinct “core–shell” structure. This molecular architecture imparts OVPOSS with exceptional thermal stability, chemical reactivity, and good compatibility with polymer matrices.

The UPR/VIPS resin system was successfully fabricated by incorporating OVPOSS into the UPR through copolymerization. On the one hand, the high bond energy of the Si–O–Si framework allows it to absorb and reflect thermal energy, thereby retarding the thermal degradation of the polymer matrix. Moreover, the rigid cage structure of OVPOSS effectively restricts the expansion of the free volume in UPR chain segments, thereby suppressing high-temperature creep. On the other hand, the vinyl functional groups on the periphery of OVPOSS can participate in free-radical polymerization reactions with the carbon–carbon double bonds of UPR, forming covalent crosslinking sites and an

interpenetrating polymer network. The synergistic combination of covalent bonding and van der Waals interactions enhances interfacial adhesion between OVPOSS and the UPR matrix, effectively suppressing phase separation and significantly improving the toughness of the resulting composite.

Fig. 2a displays the ^{1}H NMR spectrum of OVPOSS. The signals appearing in the range of 6.27–5.68 ppm are assigned to the vinyl protons (–CH═CH_2, ^{1}H, I and –CH═CH_2, ^{1}H, II), confirming the presence of vinyl functional groups on the OVPOSS molecule. The ^{29}Si NMR spectrum of OVPOSS is shown in Fig. 2b, where a single sharp peak at −80.2 ppm corresponds to the silicon chemical shift characteristic of the cage-like silsesquioxane structure. The appearance of a single, well-resolved peak indicates the high purity of the synthesized product and further verifies the successful formation of the desired OVPOSS cage framework. These observations are corroborated by the results of FTIR spectroscopy [16].

FTIR spectroscopy was employed to further characterize the chemical structures of the synthesized materials, as shown in Fig. 2c. In the FTIR spectrum of OVPOSS, the peaks at 1110 cm^{-1} and 1008 cm^{-1} are attributed to the primary and secondary Si–O–Si stretching vibrations, respectively, while the bending vibration of Si–O–Si is observed at 468 cm^{-1}. The band at 1276 cm^{-1} corresponds to the Si–C stretching vibration, and the absorption at 968 cm^{-1} is assigned to the out-of-plane bending of vinyl (C═CH) bonds. In addition, the in-plane bending of C═CH appears at 1407 cm^{-1}, and the stretching vibration of C═C is observed at 1604 cm^{-1}. The simultaneous presence of C═CH and Si–O–Si characteristic peaks confirms the successful synthesis of OVPOSS. For the UPR/VIPS resin system, the absorption band at 1727

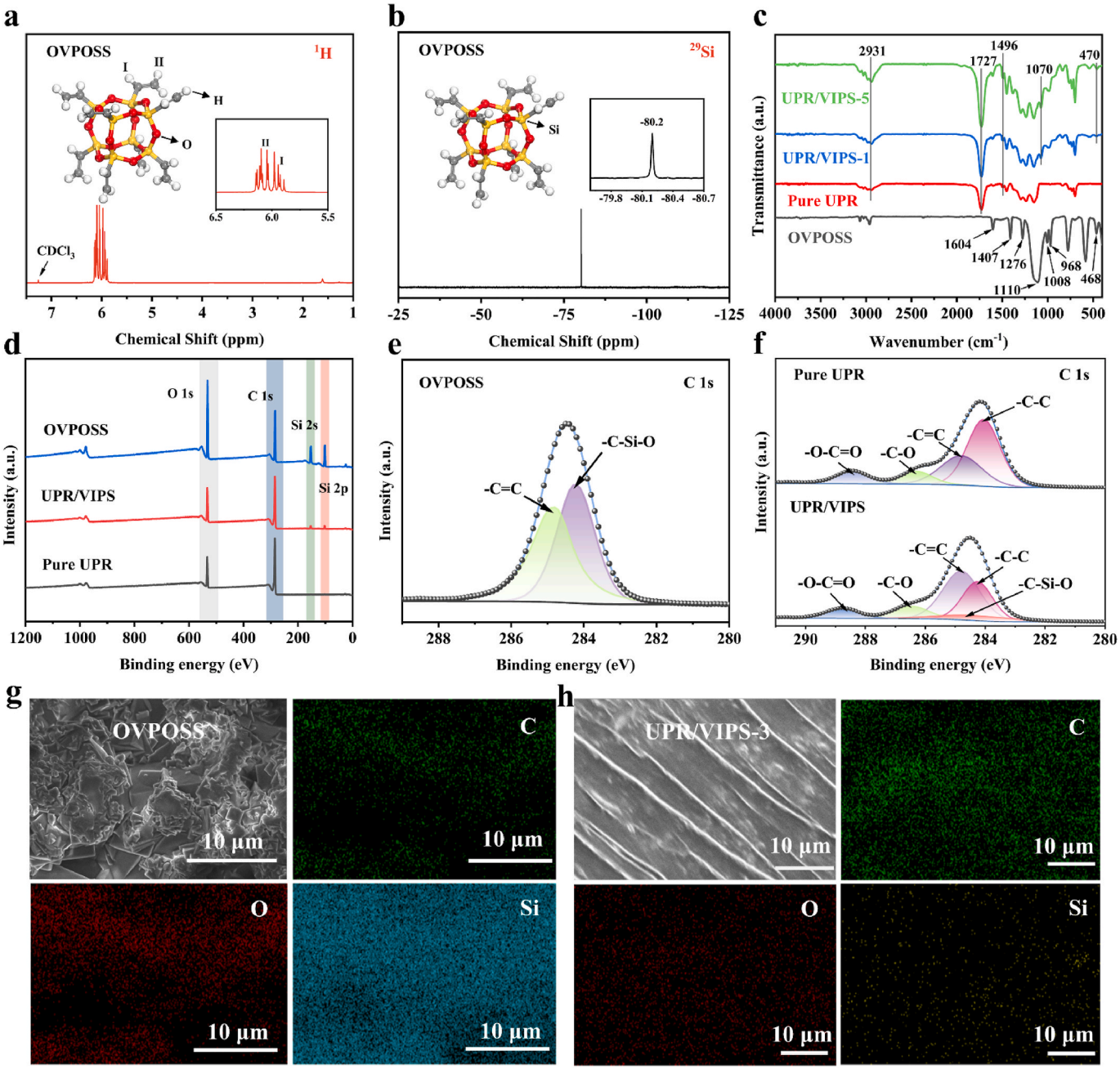

Fig. 2. a) ^{1}H NMR spectrum of OVPOSS in $CDCl_3$; b) ^{29}Si NMR spectrum of OVPOSS in $CDCl_3$; c) FTIR spectra of OVPOSS, Pure UPR resin, UPR/VIPS-1 resin, and UPR/VIPS-5 resin; d-f) High-resolution C 1s XPS spectra of OVPOSS, Pure UPR, and UPR/VIPS resin; g) SEM and elemental distribution images of OVPOSS; h) SEM and elemental distribution images of UPR/VIPS-3 resin.

cm^{-1} corresponds to the stretching vibration of the ester carbonyl (–COO–) group, indicating that hydroxyl and carboxyl groups underwent condensation to form ester bonds [22,29]. Moreover, the absorption bands at 1070 cm^{-1} and 470 cm^{-1} are assigned to the Si–O–Si stretching and bending vibrations, respectively. These characteristic peaks are absent in the spectrum of Pure UPR but become increasingly pronounced in UPR/VIPS with higher modifier content, confirming the successful incorporation of OVPOSS into the unsaturated polyester matrix. Furthermore, the absorption bands at 2931 cm^{-1} and 1496 cm^{-1} correspond to the stretching vibration of C–H linked to ester groups and the aromatic C═C stretching vibration, respectively, further validating the synthesis of the unsaturated polyester resin [37].

The chemical compositions of OVPOSS, pure UPR, and UPR/VIPS resin systems were analyzed using XPS, as shown in Fig. 2d–f and Fig. S2. In Fig. 2e, the C 1s spectrum of OVPOSS can be deconvoluted into two distinct peaks at 284.4 eV and 284.8 eV, which are assigned to –C–Si–O and –C═C bonds, respectively. As depicted in Fig. 2f, the C 1s spectra of both Pure UPR and UPR/VIPS resins exhibit four characteristic peaks located at 284.1 eV, 284.8 eV, 286.3 eV, and 288.4 eV, corresponding to –C–C bonds within phenyl rings, –C═C bonds in the polymer chains and OVPOSS, –C–O bonds, and –O–C═O ester groups, respectively. Notably, the intensity of the –C═C peak in the UPR/VIPS spectrum increases markedly, which is attributed to the introduction of vinyl groups from OVPOSS. In addition, a new peak emerges at 284.5 eV, assigned to the –C–Si–O bond, further confirming the successful incorporation of OVPOSS into the unsaturated polyester matrix. To further examine the microstructure and elemental distribution, SEM was performed on the UPR/VIPS resin, as shown in Fig. 2h. The SEM image reveals a uniform and compact morphology. Moreover, the corresponding energy-dispersive X-ray spectroscopy (EDS) and elemental mapping results (Fig. 2g–h and Fig. S3) demonstrate the presence of carbon (C), oxygen (O), and silicon (Si) in the UPR/VIPS system, verifying the successful formation of a hybrid resin network incorporating OVPOSS.

The solubility of OVPOSS is a crucial factor influencing its potential applications. As presented in Table S1 and Fig. S5, OVPOSS exhibits good solubility in tetrahydrofuran (THF), dichloromethane (DCM), and chloroform. It shows moderate solubility in dimethylformamide (DMF), dimethyl sulfoxide (DMSO), and ethyl acetate. In contrast, the solubility of OVPOSS is poor in solvents such as ethanol, methanol, and petroleum ether [38].

3.2. Model optimization

3.2.1. Density equilibration

Fig. 3b shows the time-dependent density evolution of each resin system following the final NPT simulation. All systems were initially constructed with a density of 0.95 g/cm^3. After multiple stages of dynamic equilibration, the densities increased markedly and stabilized within a fluctuation range of ±0.025 g/cm^3. The density profiles of the Pure UPR and UPR/VIPS systems clearly demonstrate that the incorporation of OVPOSS via copolymerization results in a notable increase in the equilibrium density of the resin systems.

3.2.2. Energy balance

Fig. 3c and d depict the time-dependent energy profiles of the Pure UPR and UPR/VIPS systems at 600 K. An increase in both the number of molecules and the total system energy is observed, indicating that the copolymerization of OVPOSS leads to a more compact molecular packing within the crosslinked network. This denser configuration enhances intermolecular non-bonded interactions, thereby increasing the system's non-bonded energy. Furthermore, the energy fluctuations for each system remain within 5 %, satisfying the convergence criteria and aligning with the fundamental principle that the total energy of a system is the sum of its kinetic and potential energy.

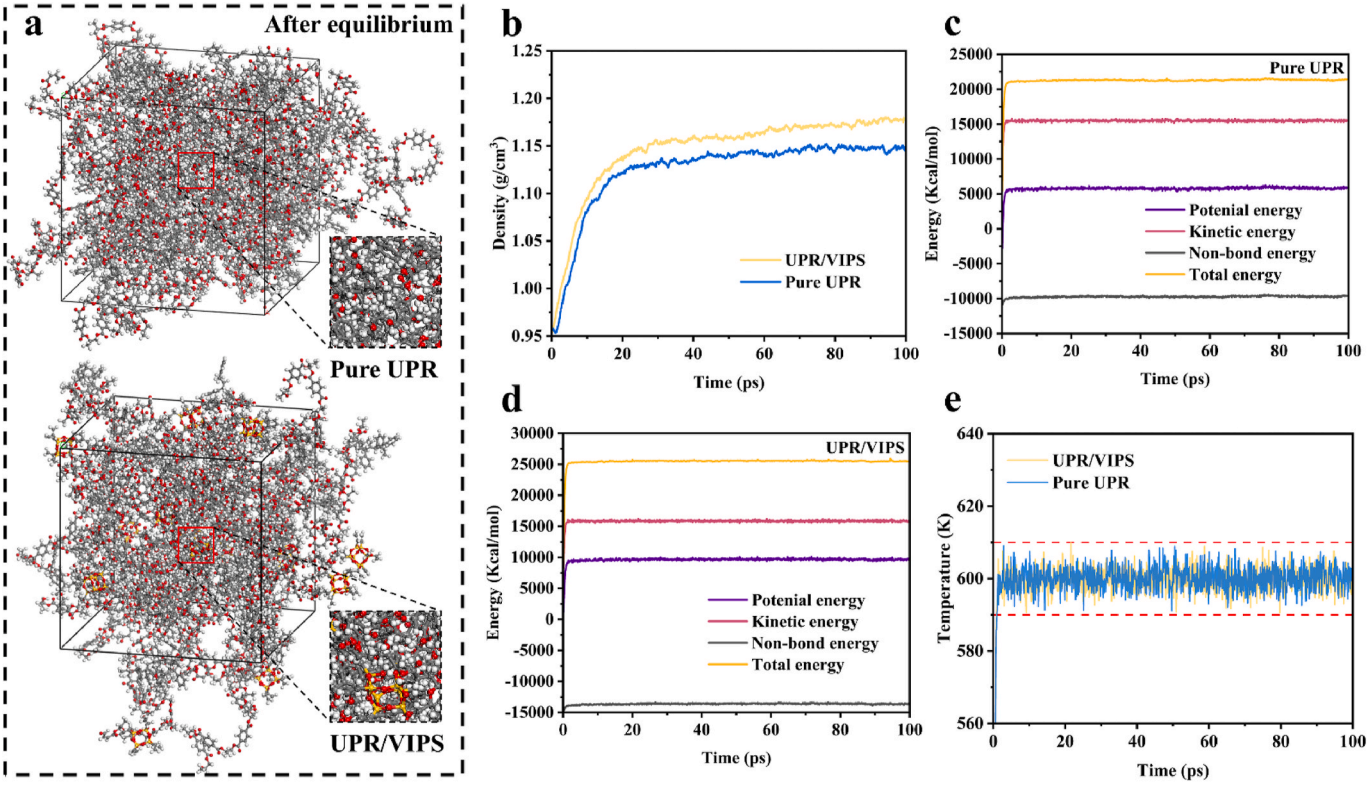

Fig. 3. a) Optimized and equilibrated model of the resin cross-linked system; in MD simulations: b) Plots of density vs. time for different resin systems at 600 K; c) Energy vs. time plot of the Pure UPR system at 600 K; d) Energy vs. time plot of the UPR/VIPS system at 600 K; e) Plots of temperature vs. time for different resin systems at 600 K.

3.2.3. Temperature equilibrium

Fig. 3e presents the temperature profiles of the different resin systems following the final NPT simulation. As shown, the temperature of each system stabilizes at approximately 600 K, with fluctuations maintained within ±15 K. At this stage, the density, total energy, and temperature of all systems have reached equilibrium, indicating that the dynamic relaxation during the 100 ps molecular dynamics simulation was successfully achieved.

3.3. Mechanical performances

3.3.1. Tensile properties

As shown in Fig. 4, the tensile properties of Pure UPR and UPR/VIPS-1 through −5 resin systems, each containing different amounts of OVPOSS, were evaluated at room temperature. Representative mechanical parameters for these systems are summarized in Table S2. According to the tensile stress–strain curves in Fig. 4a and b and the data presented in Table S2, the tensile strength of the resin systems follows an increasing trend in the order: Pure UPR < UPR/VIPS-1 < UPR/VIPS-5 < UPR/VIPS-2 < UPR/VIPS-4 < UPR/VIPS-3.

Therefore, the appropriate incorporation of POSS effectively enhances the tensile strength of the resin system, while excessive loading results in a decline in mechanical performance. Compared to the tensile strength and elongation at break of Pure UPR resin (45.04 MPa and 1.77 %, respectively) and those of other modified resin systems summarized in Table S2, the UPR/VIPS-3 resin system incorporating 1 wt% OVPOSS exhibits notably higher performance metrics, achieving 63.03 MPa and 2.98 % for the two properties, respectively. Meanwhile, the tensile modulus of the UPR/VIPS systems exhibited an overall increasing trend with increasing OVPOSS content. However, both tensile strength and elongation at break followed a non-monotonic pattern: they initially increased with OVPOSS content and subsequently decreased. Among all

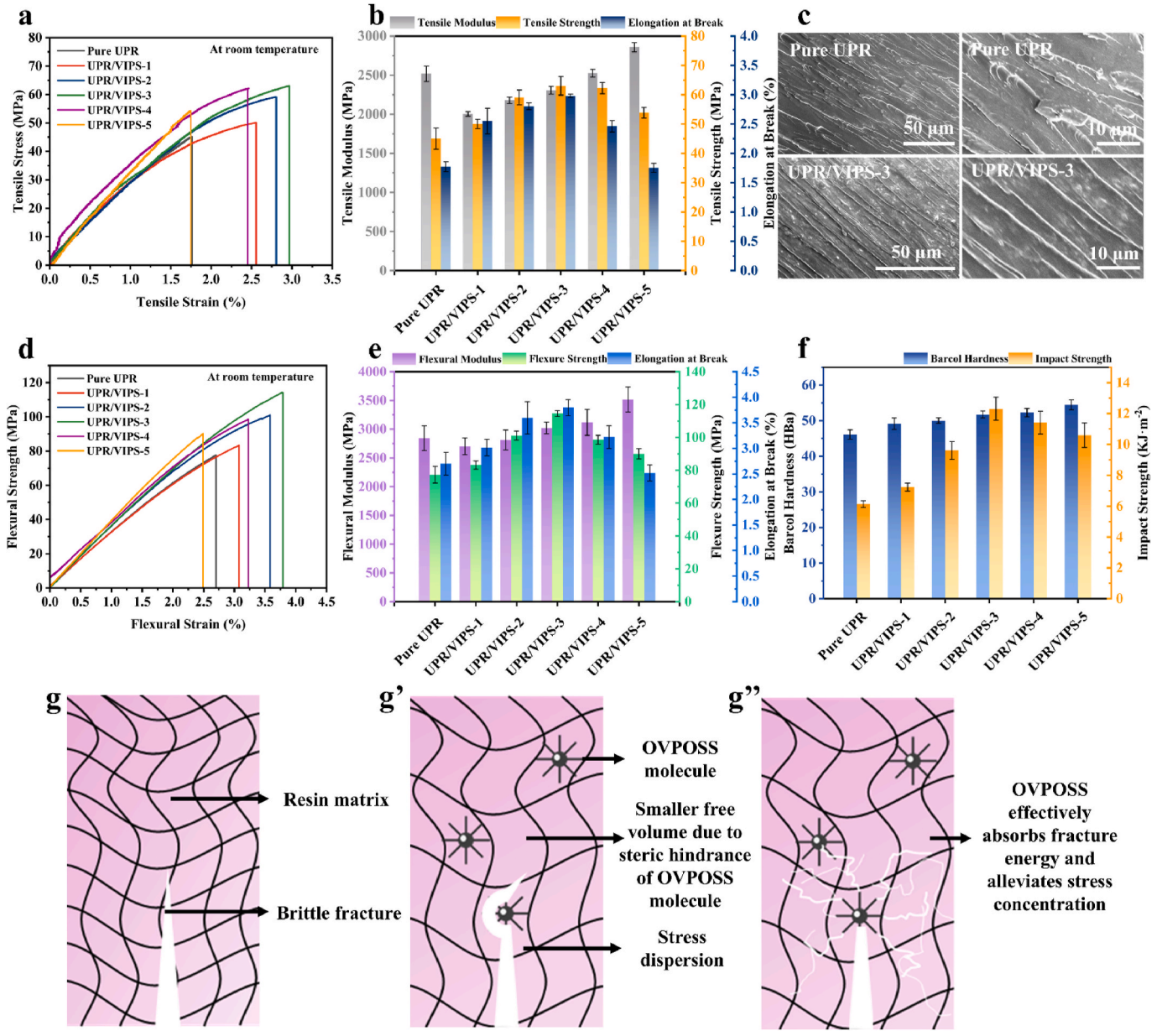

Fig. 4. a) Tensile stress-strain curves of Pure UPR and UPR/VIPS resin systems at room temperature; b) Tensile properties of resin systems with different OVPOSS contents at room temperature; c) SEM images of fracture surfaces of Pure UPR and UPR/VIPS resin systems; d) Flexural stress-strain curves of Pure UPR and UPR/VIPS resin systems at room temperature; e) Flexural properties of resin systems with different OVPOSS contents at room temperature; f) Fracture properties of resin systems with different OVPOSS contents; g-g'') Schematic illustrations of the toughening mechanism of OVPOSS.

formulations, the UPR/VIPS-3 resin system showed the highest elongation at break (2.98 %), representing a 68.4 % improvement over the Pure UPR system. These results demonstrate that the incorporation of OVPOSS has a significant impact on both tensile strength and ductility. The enhancement in elongation at break can be attributed to the copolymerization between the vinyl groups of OVPOSS and the unsaturated bonds in the UPR matrix, along with the intrinsic rigidity of the POSS cage structure. On one hand, the interpenetrating network formed by the rigid POSS cages helps relieve internal stress concentrations within the resin matrix. On the other hand, the reinforced crosslinked polymer network can dissipate applied stress through mechanisms such as chain entanglement, slippage, and rearrangement, thereby delaying crack propagation. However, at higher OVPOSS loadings, the increased system stiffness and modulus—along with enhanced steric hindrance and potential nanoparticle aggregation—lead to localized stress concentration, ultimately reducing both tensile strength and elongation at break [39,40].

As shown in Fig. 4, the elongation at break of the UPR/VIPS resin system reached 2.98 % at room temperature, compared to 1.77 % for the Pure UPR system. This enhancement is primarily attributed to the incorporation of POSS units, which are covalently grafted onto the UPR molecular chains, thereby enabling the UPR/VIPS system to absorb more energy under applied stress. These findings clearly demonstrate that the addition of OVPOSS significantly improves the toughness of the UPR/VIPS resin system at ambient conditions. Furthermore, as the OVPOSS content increases from UPR/VIPS-1 to UPR/VIPS-2 and then to UPR/VIPS-3, the elongation at break shows a corresponding progressive increase, indicating that OVPOSS exerts a positive effect on the ductility of the resin system within this concentration range.

3.3.2. Flexural properties

The flexural properties of Pure UPR and UPR/VIPS resin systems with varying OVPOSS contents at room temperature are presented in Fig. 4d, and the corresponding mechanical parameters are summarized in Table S3. The flexural strength follows the order: Pure UPR < UPR/VIPS-1 < UPR/VIPS-5 < UPR/VIPS-4 < UPR/VIPS-2 < UPR/VIPS-3. As shown in Fig. 4d and e, the flexural modulus of Pure UPR and UPR/VIPS-3 reached 2844 MPa (2.84 GPa) and 3021 MPa (3.02 GPa), respectively, indicating that the incorporation of OVPOSS effectively enhances the stiffness of the resin system. Additionally, all UPR/VIPS systems exhibited significantly higher flexural strength than the Pure UPR system.

With increasing OVPOSS content, the flexural strength of the UPR/VIPS systems initially increased and then decreased. The maximum flexural strength of 114.58 MPa was achieved by the UPR/VIPS-3 system containing 1 wt% OVPOSS, corresponding to a 48.2 % improvement compared to Pure UPR. This enhancement is primarily attributed to the unique organic–inorganic hybrid structure of OVPOSS. The vinyl groups on the organic periphery participate in free-radical copolymerization with the UPR, forming strong covalent linkages, while the rigid silsesquioxane core serves to absorb fracture energy and inhibit crack propagation. As a result, the polymer network becomes more densely crosslinked, increasing its cohesive energy and consequently improving its flexural performance. Moreover, the incorporation of OVPOSS introduces nanoscale rigid domains into the UPR matrix, which can promote localized stress redistribution and facilitate plastic deformation, thereby improving the moldability and damage tolerance of the resin. These findings demonstrate that OVPOSS not only reinforces but also toughens the flexural behavior of UPR-based composite systems.

3.3.3. Fracture toughness

The variations in Barcol hardness and impact strength of Pure UPR and UPR/VIPS resin systems at room temperature are presented in Fig. 4f, with the corresponding values summarized in Table S4. As shown in Fig. 4f, the Barcol hardness of the resin systems increases progressively with increasing OVPOSS content, while the impact strength exhibits a non-monotonic trend, initially increasing and subsequently decreasing. Both the Barcol hardness and impact strength of the UPR/VIPS systems (51.72 HBa and 12.31 kJ m^{-2}, respectively) are significantly higher than those of the Pure UPR system. Notably, when the OVPOSS content reaches 1 wt%, the UPR/VIPS resin system shows marked enhancements in both properties, with increases of 12.2 % in hardness and 100.7 % in impact strength compared to the Pure UPR. These improvements can be primarily attributed to the introduction of OVPOSS, which enhances the matrix's plastic deformation capability under dynamic loading. The rigid silsesquioxane cages facilitate stress transfer and promote shear yielding in the resin matrix, thereby increasing its energy dissipation capacity. However, at higher OVPOSS loadings, the impact strength begins to decline. This reduction is likely caused by the steric hindrance and aggregation of OVPOSS nanoparticles, which induce localized stress concentrations that facilitate crack initiation and propagation, ultimately compromising the impact resistance of the system.

Among the tested formulations, the UPR/VIPS-3 resin system exhibited the best toughening performance, which can be attributed to the synergistic effects of chemical copolymerization and physical blending between OVPOSS and the unsaturated polyester matrix. In addition, as shown in Fig. 4c and Fig. S6, SEM images of the fracture surfaces of Pure UPR and UPR/VIPS resin systems revealed distinct differences. Under external loading, insufficient energy dissipation in Pure UPR led to premature crack initiation and brittle fracture, consistent with the schematic illustration in Fig. 4g. In contrast, the UPR/VIPS samples exhibited pronounced stress whitening and a more uniform texture, indicating enhanced energy dissipation during fracture.

The toughening mechanisms of the UPR/VIPS system under external stress are further illustrated in Fig. 4g′ and g″. On one hand, the applied stress is redistributed around the rigid cage-like POSS structures, leading to a more homogeneous stress distribution within the polymer matrix. This stress delocalization suppresses the initiation and propagation of microdefects and cracks, thereby improving the load-bearing capacity of the material prior to failure. The covalent copolymerization and physical entanglement between OVPOSS and the polymer chains further reinforce the matrix structure. On the other hand, under high-impact loading conditions, OVPOSS can act as a rigid nanoscale core that debonds from the surrounding matrix. This debonding process absorbs a large amount of mechanical energy, thereby delaying catastrophic failure (e.g., transient brittle fracture, sudden fracture under alternating stress, and overall fragmentation). Such an energy dissipation mechanism is widely recognized as a key toughening contributor in silane-modified nanocomposite systems [41–44].

Furthermore, the incorporation of vinyl-functionalized OVPOSS introduces additional Si–O bonds and reactive vinyl groups, which not only improve the compatibility between organic and inorganic phases but also facilitate the formation of a more uniform microstructure. The coexistence of rigid inorganic cores and a densely crosslinked polymer network effectively balances stiffness and toughness. These combined effects enhance the plastic deformation capacity and crack resistance of the resin system, ultimately improving its overall fracture toughness.

3.3.4. Mechanical property simulation

To further elucidate the modification mechanism of OVPOSS on UPR, MD simulations were conducted to investigate its influence on the molecular structure and mechanical behavior of UPR. By analyzing the internal forces and strain responses during simulated deformation, the mechanical parameters of the resin systems were quantitatively determined. The mechanical properties were calculated using the static constant strain method implemented in the Forcite module. In this method, shear deformations were systematically applied to the three-dimensional resin models along the *xx*, *yy*, *zz*, *yz*, *xz*, and *xy* planes, which correspond to the *11*, *22*, *33*, *23*, *13*, and *12* components of the strain tensor, respectively. The resulting stress–strain behavior follows Hooke's law, which is represented in matrix form in Equation (1), where

C_{ij} denotes the elastic stiffness coefficients, σ_i is the applied stress (maintained below 0.01), and ε_j is the resulting strain. Since UPR can be reasonably approximated as an isotropic material, the stiffness matrix simplifies to matrix S(2), in which λ and μ are the Lamé constants. These constants were calculated using Equations (2) and (3):

$$\lambda = \frac{1}{3}\left(C_{11} + C_{22} + C_{33}\right) - \frac{1}{3}\left(C_{44} + C_{55} + C_{66}\right) \tag{2}$$

$$\mu = \frac{1}{3}\left(C_{44} + C_{55} + C_{66}\right) \tag{3}$$

The Young's modulus (E), shear modulus (G), bulk modulus (B), and Poisson's ratio (ν) of the resin system are calculated according to the following equations:

$$E = \mu \times \frac{3\lambda + 2\mu}{\lambda + \mu} \tag{4}$$

$$G = \mu \tag{5}$$

$$B = \lambda + \frac{2}{3}\mu \tag{6}$$

$$\nu = \frac{\lambda}{2(\lambda + \mu)} \tag{7}$$

As shown in Fig. 5a–c, under identical crosslinking degrees, the UPR/VIPS system exhibits superior mechanical performance compared to the Pure UPR system. The incorporation of OVPOSS leads to increases in shear modulus, Young's modulus, and bulk modulus. Fig. 5d shows that the Poisson's ratio remains nearly constant for both systems, fluctuating around 0.34. Additionally, Fig. 5a–c reveal that the Young's modulus, shear modulus, and bulk modulus of both the Pure UPR and UPR/VIPS systems decrease with increasing temperature. However, beyond 500 K, the rate of mechanical property degradation becomes less pronounced.

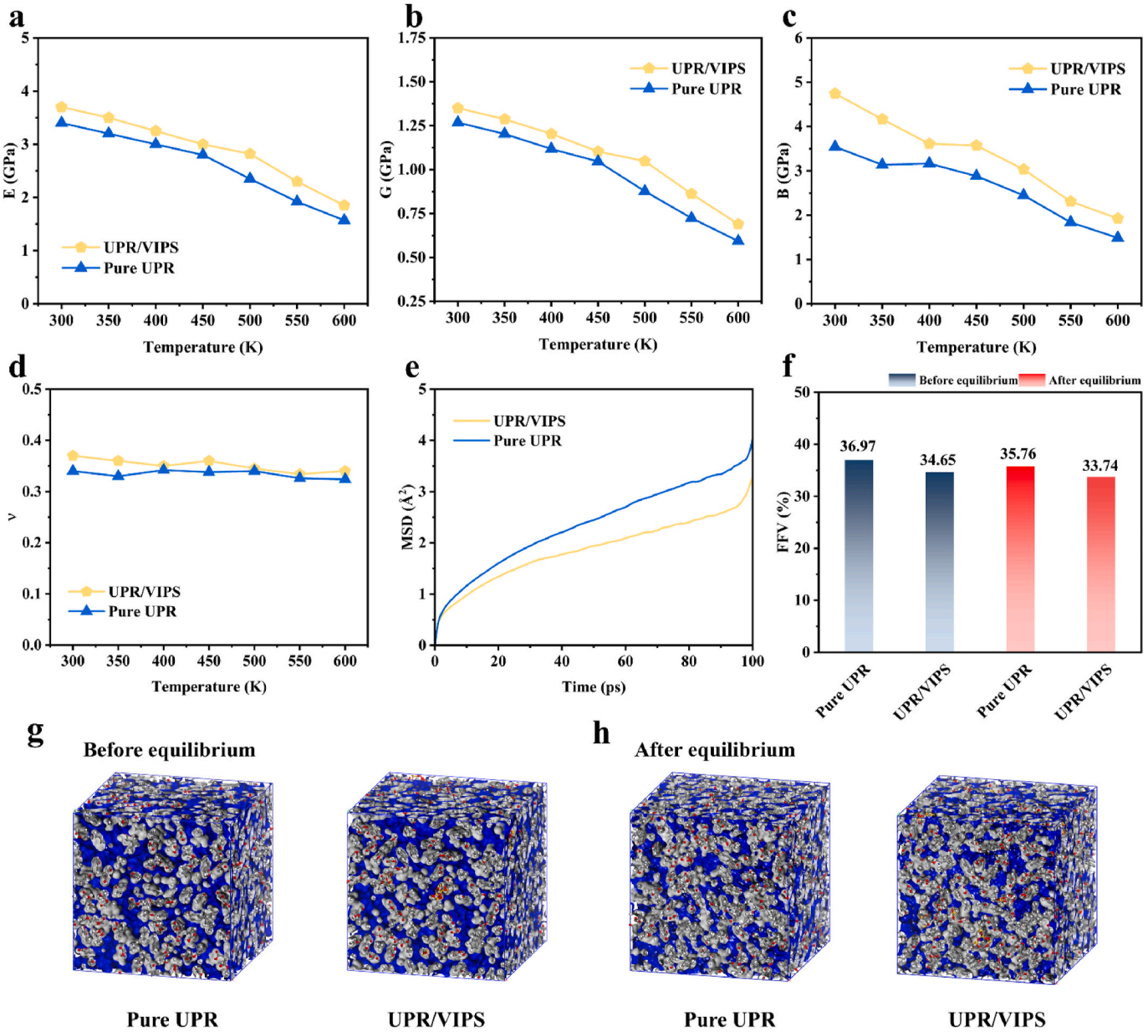

Fig. 5. In MD simulations: a) Young's moduli of different resin systems; b) Shear moduli of different resin systems; c) Bulk moduli of different resin systems; d) Poisson's ratios of different resin systems; e) Mean square displacements of different resin systems; f) FFV of different resin systems before and after optimization and equilibration; g-h) Connolly surface models of different cross-linked systems before and after optimization and equilibration.

Notably, the Pure UPR system exhibits the most rapid decline between 450 and 500 K, while the UPR/VIPS system experiences its steepest decrease between 500 and 550 K. This trend is attributed to the fact that mechanical properties deteriorate most significantly near the T_g, confirming that the incorporation of nanofillers effectively elevates the T_g of the resin system. Overall, the introduction of nanomaterials into UPR systems significantly enhances their mechanical properties. OVPOSS plays a key role in this enhancement due to its unique inorganic cage-like core and organic functional shell. The copolymerization between the vinyl groups on OVPOSS and the unsaturated moieties in the UPR molecular chains reduces the free volume within the system. Moreover, the rigid inorganic cage structure restricts molecular chain mobility, thereby improving the tensile and shear performance of the composite resin system [45–48].

3.4. Characterization of chain segment motion

The mean square displacement (MSD) is a key metric used in MD simulations to quantify the positional changes of atoms over time, thereby reflecting the mobility of polymer chains. In this study, the MSD values of the two resin systems were calculated using the Forcite module. As illustrated in Fig. 5e, the incorporation of OVPOSS significantly reduces the MSD, indicating a marked restriction in the mobility of polymer chain segments. This reduction suggests that the presence of nanofillers effectively suppresses the thermal Brownian motion of molecules in the unsaturated polyester resin system. As a result, the segmental motion is constrained, which theoretically corresponds to an increase in the T_g. Fig. 5e clearly shows that, under identical crosslinking conditions, the MSD of the Pure UPR system is substantially higher than that of the UPR/VIPS system. This discrepancy is primarily attributed to the absence of nanomaterial reinforcement in the Pure UPR, allowing greater internal molecular motion. In contrast, the OVPOSS-containing UPR/VIPS system exhibits reduced chain mobility due to the rigid cage-like structure of OVPOSS, which physically restricts segmental dynamics and enhances the thermal and mechanical stability of the resin network.

3.5. Free volume

The concept of free volume, originally proposed by Fox and Flory, divides the total volume of a material into two components: the occupied volume (V_o) and the free volume (V_t). V_o corresponds to the space physically occupied by the resin molecules, whereas V_t represents the voids within the system that facilitate molecular motion. The fractional free volume (FFV), defined as the ratio of V_t to the total system volume, is calculated according to Equation (8).

$$\mathrm{FFV} = \frac{V_t}{V_t + V_0} \times 100\% \tag{8}$$

To evaluate the FFV, Connolly surfaces of the resin systems with varying crosslinking degrees were constructed using the Atom Volume and Surface module in the Materials Studio (MS) software. These structures were analyzed before and after geometric optimization and dynamic equilibration. Subsequently, the systems were cooled from 600 K to 300 K in 20 K intervals to simulate thermal relaxation. The free volume distributions of the optimized and equilibrated crosslinked systems are presented in Fig. 5g and h. Free volume refers to the intermolecular voids within the polymer matrix, which form spatially distinct structures. In Fig. 5g and h, the blue and gray regions correspond to the interior and surface of the free volume, respectively, clearly delineating the three-dimensional topology of the void spaces.

Fig. 5f illustrates that the FFV of the resin system decreases significantly upon the incorporation of OVPOSS. This reduction is primarily attributed to the high density of unpaired surface atoms on the OVPOSS nanoparticles, which elevates the local electron density within the amorphous regions and effectively reduces the available free volume. A comparative analysis of the systems before and after optimization and equilibration underscores the crucial role of MD relaxation and highlights the substantial impact of OVPOSS on lowering the FFV in crosslinked networks. The Pure UPR system contains a high concentration of ester linkages, which impart considerable flexibility to the polymer chains. This flexibility promotes chain torsion and conformational variability, thereby increasing the FFV and potentially compromising certain mechanical and thermal properties. With the introduction of OVPOSS, the nanoparticles actively participate in the crosslinking polymerization of the unsaturated polyester matrix. In addition, resin chains can penetrate the rigid inorganic cage structure of OVPOSS, forming strong intermolecular interactions. These interactions increase the occupied volume within the system, leading to a corresponding reduction in free volume and FFV. These findings clearly demonstrate that OVPOSS effectively reduces the FFV of the resin system. The synergistic effect of the rigid silsesquioxane cage core and the reactive organic substituents on OVPOSS facilitates copolymerization and network densification. This dual contribution is chiefly responsible for the pronounced reduction in FFV and the subsequent enhancement of the overall performance of the UPR/VIPS composite system.

3.6. Cohesive energy

The cohesive energy density (CED) characterizes the strength of intermolecular interactions among functional groups within the resin system. A higher CED value signifies stronger and more stable interactions between polymer chains, reflecting the material's overall structural integrity. CED is defined as the cohesive energy per unit volume and can be quantitatively expressed by the following equation:

$$\mathrm{CED} = \frac{\Delta E}{\nu} \tag{9}$$

here, ν denotes the molar volume.

A higher CED indicates tighter intermolecular packing and stronger intermolecular interactions. As summarized in Table 1, the incorporation of OVPOSS effectively enhances both van der Waals and Coulombic interactions within the UPR system. Compared with the Pure UPR, the introduction of OVPOSS leads to a marked increase in CED, confirming the reinforcing effect of the nanomaterial on the polymer network.

3.7. Thermal stability and dielectric properties

3.7.1. Glass transition temperature

The glass transition temperature (T_g) defines the upper limit of the service temperature for UPR and plays a critical role in determining its mechanical performance [48,50]. In this study, the Anneal function in the Forcite module was employed to perform thermal annealing on various resin systems. Each system subsequently underwent two 100 ps MD equilibration steps under the NPT ensemble at varying temperatures. The pressure was maintained at 0.0001 GPa, and the temperature was decreased stepwise from 600 K to 300 K in 20 K intervals. The first equilibration stage served to eliminate local residual stresses and ensure equilibrium in both volume and density. The second stage was used to record system parameters such as density and temperature throughout the cooling process. Based on the collected temperature–density data, density–temperature curves were constructed for each system. The glass transition temperature was determined by applying bilinear fitting to

Table 1
Cohesion energy density of different resin systems.

Resin Code	CED (J/m^3)			
	Total	Van der Waals	Electrostatic	Other
Pure UPR	3.05E+08	2.61E+08	2.59E+07	1.82E+07
UPR/VIPS	3.18E+08	2.74E+08	2.60E+07	1.80E+07

the density–temperature scatter plots. The temperature corresponding to the intersection of the two fitted lines was defined as the T_g [49–51].

The T_g of UPR is primarily determined by the internal free volume and the rigidity of the molecular chains, both of which can be characterized by the MSD. An increase in free volume generally results in a decrease in T_g, whereas a reduction in MSD indicates restricted molecular thermal motion, thereby leading to an increase in T_g. As shown in Fig. 6a, the temperature–density curves obtained from MD simulations yield T_g values of 449 K (175.9 °C) for Pure UPR and 486 K (212.9 °C) for the UPR/VIPS system. Correspondingly, Fig. 6c presents the DSC results, where the T_g values of Pure UPR and the UPR/VIPS-5 system are 137.7 °C and 165.1 °C, respectively. These results demonstrate that the copolymerization of OVPOSS reduces the mobility of molecular chains, while the rigid Si–O–Si cage structure increases steric hindrance, thereby restricting chain rotation and molecular thermal motion. It should also be noted that, in simulations, factors such as model construction, matrix selection, crosslinking methodology, and annealing rate can influence the predicted T_g, often resulting in values higher than those obtained experimentally. Nevertheless, the overall trends observed in simulations are consistent with experimental results, confirming that the incorporation of OVPOSS enhances the T_g of UPR.

Thermogravimetric analysis (TGA) was conducted to further evaluate the thermal stability of the various UPR systems, as shown in Fig. 6d and e. The results clearly demonstrate that the incorporation of an appropriate amount of OVPOSS enhances the initial decomposition temperature ($T_{d5\ \%}$) of the resin, thereby improving its thermal resistance. Specifically, the $T_{d5\ \%}$ values for UPR/VIPS-5 and UPR/VIPS-3 are 292.1 °C and 297.5 °C, respectively, representing increases of 17.5 °C and 22.9 °C compared to that of Pure UPR. In addition, the thermal index temperatures (T_s) for UPR/VIPS-5 and UPR/VIPS-3 reach 164.5 °C and 168.2 °C, corresponding to improvements of 8.1 °C and 11.8 °C, respectively, over the Pure UPR system (see Table 2). The improved thermal stability is primarily attributed to the rigid inorganic cage-like structure of OVPOSS and the presence of high-bond-energy Si–O and Si–C bonds, which are known to contribute significantly to thermal resistance. However, when the OVPOSS content exceeds an optimal threshold—as in the case of UPR/VIPS-5—aggregation of POSS nanoparticles may occur, thereby limiting their ability to form effective chemical bonds with the UPR matrix. Furthermore, excessive inorganic content can lead to phase separation and reduced crosslinking efficiency, ultimately compromising the overall thermal stability of the resin system [52–55].

Fig. 6d presents the TGA curves of the Pure UPR and UPR/VIPS systems. Compared to the Pure UPR, the incorporation of OVPOSS significantly elevates the decomposition temperature (T_d). At an OVPOSS content of 1 wt%, the $T_{d5\ \%}$ and char yield reach their maximum values of 297.5 °C and 9.6 %, respectively. However, further increases in OVPOSS content result in a decline in both $T_{d5\ \%}$ and char yield, which may be attributed to enhanced molecular chain mobility within the resin system. The unique cage-like structure of OVPOSS, coupled with its covalent integration into the polymer network, effectively reduces the free volume and restricts the segmental motion of polymer chains. This constraint on molecular mobility is particularly evident in the increase of the T_g, which reaches 158.2 °C at the optimal OVPOSS concentration. Additionally, the temperature–density curve becomes smoother, indicating a more thermodynamically stable network structure. These synergistic effects collectively contribute to the improved thermal stability of the nanocomposite resin system.

3.7.2. Thermal deformation behavior

Fig. 6f presents the thermal deformation curves of various resin systems, with the corresponding data summarized in Table 2. The thermal stability of each sample was assessed by measuring deformation under increasing temperatures. The thermal deformation temperature (T_{HDT}), defined as the temperature at which a deformation of 0.35 mm is observed, progressively increases with the incorporation of OVPOSS. As a critical indicator of a material's dimensional stability under thermal stress, a higher T_{HDT} reflects superior resistance to heat-induced deformation. Notably, the UPR/VIPS-3 system exhibits a T_{HDT} of 117.2 °C, representing a 25.8 % improvement over that of the Pure UPR system (93.2 °C). This enhancement is primarily attributed to the increased crosslinking density and the formation of an interpenetrating polymer network induced by OVPOSS incorporation. As shown in Fig. 6f, the Pure UPR system undergoes rapid deformation beyond 80 °C, indicating poor resistance to thermal softening. In contrast, the UPR/VIPS systems exhibit a more gradual deformation profile with rising temperature, demonstrating enhanced structural integrity at elevated temperatures. This improved thermal performance arises from the rigid Si–O–Si cage-like architecture of OVPOSS, which provides nanoscale reinforcement and maintains mechanical rigidity under thermal stress. The vinyl functional groups on OVPOSS enable covalent copolymerization with the UPR matrix, forming a densely crosslinked network that limits the expansion of free volume and suppresses segmental mobility at high temperatures. Additionally, the homogeneous dispersion of OVPOSS nanoparticles contributes to delayed thermal degradation by extending the thermal conduction pathways and leveraging the high bond energy of the Si–O–Si framework.

3.7.3. Dielectric properties

To investigate the dielectric mechanism of the resin systems, dielectric constant measurements were carried out on Pure UPR and UPR/VIPS resins at different frequencies, as shown in Fig. 6g. Within the external field range of 0.1–50 MHz, the dielectric constant of the resin systems decreased progressively with increasing OVPOSS content. This reduction is mainly attributed to the copolymerization of OVPOSS, in which the non-polar Si–O–Si cage forms rigid crosslinking sites within the UPR molecular chains. On the one hand, these crosslinking sites significantly enhance intermolecular interactions (Table 1), and on the other hand, they restrict chain rotation and segmental mobility, thereby reducing the ability of polar units (e.g., ester groups) to reorient under an external electric field and leading to diminished dipole polarization. In addition, compared with the Pure UPR system, the incorporation of the non-polar OVPOSS cage occupies part of the excess FFV in Pure UPR, further limiting the mobility of polar groups and suppressing dipole polarization, which indirectly contributes to the reduction in dielectric constant [56].

Furthermore, density functional theory (DFT) calculations were performed to analyze the electrostatic potential (ESP) and the highest occupied molecular orbital–lowest unoccupied molecular orbital (HOMO–LUMO) distributions of the structural units. As shown in Fig. 6j, the ESP maps of Pure UPR and UPR/VIPS exhibit negative potential regions (blue and white). In UPR/VIPS, non-coplanar structures are mainly distributed in these negative regions, altering the local electronic distribution and reducing the electrostatic potential in certain areas. As presented in Fig. 6k, the abundant non-coplanar structures introduced by OVPOSS cause the HOMO and LUMO orbitals of UPR/VIPS to localize predominantly at the copolymerization sites between OVPOSS and UPR, while also producing a relatively larger energy gap (E_g). A wider E_g effectively suppresses the formation of charge-transfer complexes (CTCs), thereby reducing the dipole moment, which may further contribute to lowering the dielectric constant [57–60]. Overall, these results, supported by both experimental characterization and molecular simulations, demonstrate the structural and functional advantages of the UPR/VIPS resin system over Pure UPR.

3.8. Comprehensive properties of the UPR/VIPS resin system

The overall performance of the Pure UPR and UPR/VIPS resin systems is presented in Fig. 6h and Fig. S7. As shown in Fig. 6h, the UPR/VIPS-3 formulation exhibits markedly superior comprehensive properties. Compared with the Pure UPR system, UPR/VIPS-3 shows significant improvements in tensile strength, flexural strength, HDT, impact

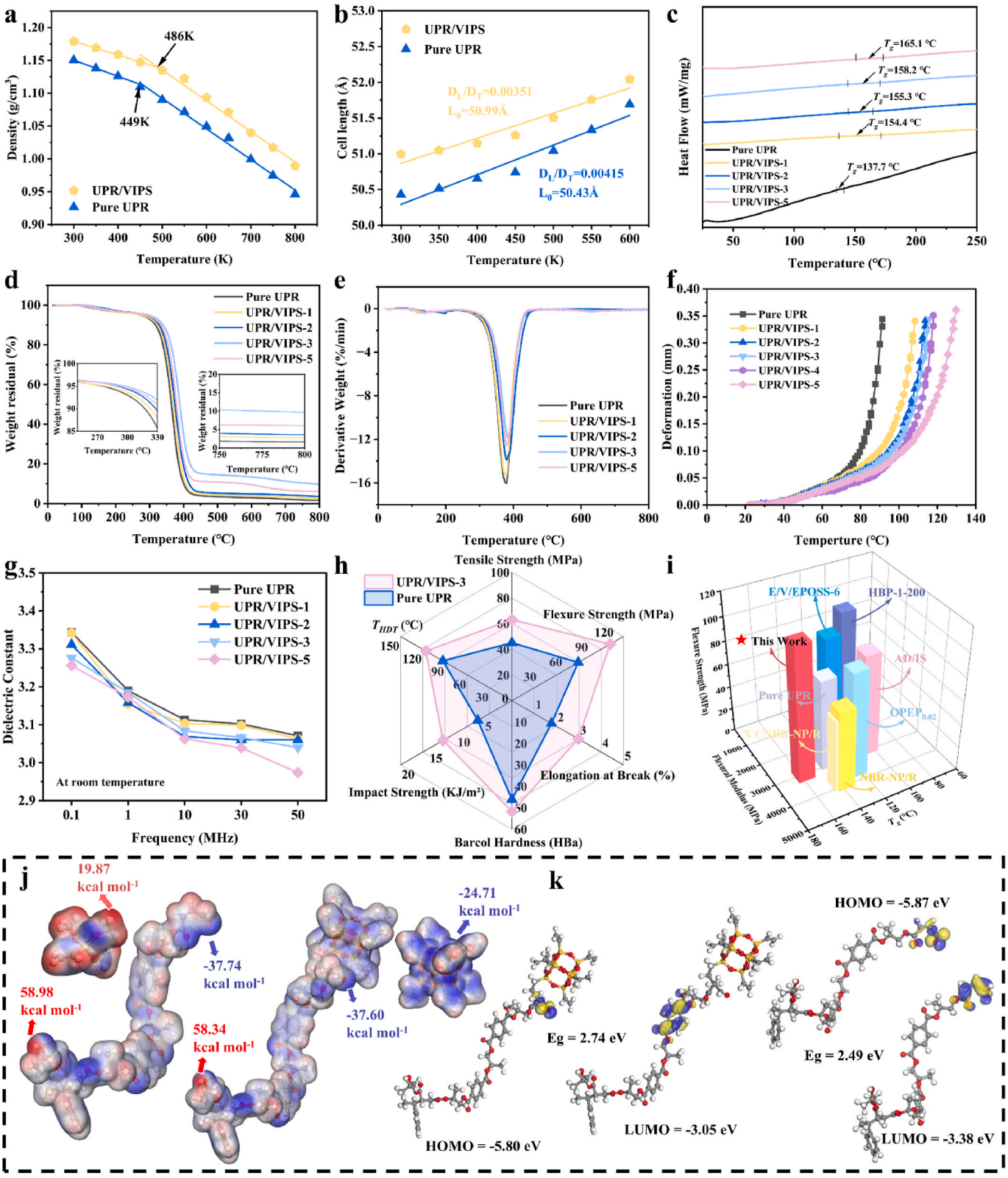

Fig. 6. a) Density vs. temperature curves of different resin systems; b) Unit cell length vs. temperature curves of different resin systems; c) DSC curves, d) TGA curves, e) DTG curves, and f) Thermal deformation curves of Pure UPR and UPR/VIPS resin systems; g) Variation of dielectric constants of different resin systems with frequency at room temperature; h) Tensile strength, flexural strength, heat distortion temperature, and other properties; i) Compares the mechanical properties and T_g of different materials, and highlights the improvements achieved in this work; j) Electrostatic potential maps of VTMS, Pure UPR, UPR/VIPS and OVPOSS; k) HOMO/LUMO orbitals of UPR/VIPS and Pure UPR.

Table 2
Summary of thermal stability performance of pure UPR and UPR/VIPS resin systems.

System	T_{HDT}[a] (°C)	$T_{d5\ \%}$[b] (°C)	$T_{d10\ \%}$[b] (°C)	T_S[b] (°C)	$T_{d30\ \%}$[b] (°C)	T_{dmax}[b] (°C)	Char yield[b] (%)
Pure UPR	93.2	274.6	315.7	156.4	348.9	375.3	1.6
UPR/VIPS-1	108.3	277.4	322.9	158.8	355.1	378.3	2.8
UPR/VIPS-2	113.8	290.1	328.1	162.6	359.6	380.3	3.7
UPR/VIPS-3	117.2	297.5	339.7	168.2	374.0	383.3	9.6
UPR/VIPS-5	129.7	292.1	333.1	164.5	364.9	381.9	6.1

[a] Obtained from VICAT HDT.
[b] Obtained from TGA, $T_s = 0.49 \times [T_{d5\ \%} + 0.6 \times (T_{d30\ \%} - T_{d5\ \%})]$.

strength, and elongation at break. In addition, Fig. S7 indicates that the viscosity of the UPR/VIPS-3 system at both 25 °C and 60 °C is slightly higher than that of the Pure UPR resin, which may be attributed to the interaction between the polymer matrix and the rigid OVPOSS nanostructure. Moreover, the tensile modulus, T_g, and $T_{d5\ \%}$ also exhibit varying degrees of enhancement, further confirming the beneficial role of OVPOSS in improving thermal and mechanical performance. Fig. 6i compares the mechanical properties and T_g of this work with those reported in previous studies, demonstrating the application potential and superiority of the present system. In summary, the incorporation of OVPOSS effectively balances the trade-off between toughness and thermal stability in UPR, offering a valuable reference for the design and development of high-performance UPR materials.

4. Conclusion

In this study, a novel strategy was developed for modifying UPR by incorporating OVPOSS into the resin matrix via copolymerization. This approach simultaneously enhances the toughness and thermal stability of the resin by leveraging the unique properties of POSS-based nanostructures, with the underlying mechanism validated through MD simulations. OVPOSS, featuring high reactivity with the UPR matrix, was successfully synthesized via an alkyl hydration reaction, and its structure was confirmed by NMR, XPS, and FTIR analyses. The FTIR and EDS results further demonstrated the uniform dispersion of OVPOSS within the resin matrix and its covalent integration into the polymer network via copolymerization with UPR chains. Unlike conventional modification strategies, this study combines molecular simulations with experimental characterization to systematically explore structure–property relationships from both theoretical and practical perspectives. At an optimal OVPOSS content of 1 wt%, the modified resin exhibits a maximum impact strength of 12.3 kJ m^{-2}, tensile strength of 63.03 MPa, and elongation at break of 3 %, representing increases of 100.6 %, 39.9 %, and 68.4 %, respectively, compared to unmodified UPR. It is noteworthy that the T_g, $T_{d5\ \%}$, and T_{HDT} increased to 158.2 °C, 297.5 °C, and 117.2 °C, representing improvements of 14.9 %, 8.3 %, and 25.8 %, respectively. Overall, this work provides a promising route for developing high-toughness, thermally stable UPR materials by employing reactive organic–inorganic hybrid nanostructures such as POSS to simultaneously improve mechanical and thermal performance. The resulting UPR/VIPS resins exhibit excellent comprehensive properties and show considerable potential for industrial applications. However, it is undeniable that the current synthesis process of OVPOSS is relatively sophisticated and costly, which to some extent limits large-scale industrial production. At the same time, this also represents a direction for our future research. Furthermore, the integrated strategy of molecular design, synthesis, and simulation presented herein offers a valuable framework for the development of functionalized POSS and their application in advanced polymer composites. Looking forward, we anticipate that future studies will increasingly incorporate artificial intelligence (AI) and molecular dynamics simulations into the rational design, structural optimization, and performance prediction of polymeric materials. In the near future, more refined and accurate methodologies are expected to emerge for analyzing and tailoring polymer structures, thereby driving innovation in high-performance resin systems.

CRediT authorship contribution statement

Chunlong Li: Writing – original draft, Validation, Methodology, Investigation, Data curation. **Mengdan Di:** Validation, Project administration. **Huige Wei:** Supervision, Project administration. **Kangfu Sun:** Methodology. **Jingguo Cao:** Writing – review & editing, Resources, Project administration, Funding acquisition.

Declaration of competing interest

The authors declare that they have no known competing financial interests or personal relationships that could have appeared to influence the work reported in this paper.

Appendix A. Supplementary data

Supplementary data to this article can be found online at https://doi.org/10.1016/j.polymer.2025.129241.

Data availability

Data will be made available on request.

References

[1] E.M. Ezeh, Advances in the development of polyester resin composites: a review, World J. Eng. 21 (2) (2024) 203–220, https://doi.org/10.1108/WJE-12-2023-0517.
[2] A. Mohammad, K. Behzad, Synthesis and characterization of a novel unsaturated polyester nanocomposite incorporating graphene oxide, DCPD maleate and Poly (MMA-BuA), Polym. Sci. B 65 (6) (2024) 914–924, https://doi.org/10.1134/S1560090423600109.
[3] Y. Guo, Q. Yang, S. Huo, J. Li, P. Jafari, Z. Fang, P. Song, H. Wang, Recyclable fire-retardant bio-based thermosets: from molecular engineering to performances and applications, Prog. Polym. Sci. 162 (2025) 101935, https://doi.org/10.1016/j.progpolymsci.2025.101935.
[4] N. Bing, J. Yang, H. Gao, H. Xie, W. Yu, Unsaturated polyester resin supported form-stable phase change materials with enhanced thermal conductivity for solar energy storage and conversion, Renew. Energy 173 (2021) 926–933, https://doi.org/10.1016/j.renene.2021.04.033.
[5] M.A. Kashfipour, N. Mehra, J. Zhu, A review on the role of interface in mechanical, thermal, and electrical properties of polymer composites, Adv. Compos. Hybrid Mater. 1 (3) (2018) 415–439, https://doi.org/10.1007/s42114-018-0022-9.
[6] H.P. Fang, Y.M. Li, D.P. Zhu, Y. Deng, D.Y. Wang, A novel P-N structure modified halloysite nanotube for simultaneously enhancing flame retardancy and mechanical properties of unsaturated polyester resin, Polym. Degrad. Stabil. 237 (2025) 111324, https://doi.org/10.1016/j.polymdegradstab.2025.111324.
[7] S. Akbari, A. Root, M. Skrifvars, S.K. Ramamoorthy, D. Åkesson, Novel bio-based branched unsaturated polyester resins for high-temperature applications, J. Polym. Environ. 32 (5) (2024) 2031–2044, https://doi.org/10.1007/s10924-023-03112-5.
[8] J.J. Chruściel, E. Leśniak, Modification of epoxy resins with functional silanes, polysiloxanes, silsesquioxanes, silica and silicates, Prog. Polym. Sci. 41 (2015) 67–121, https://doi.org/10.1016/j.progpolymsci.2014.08.001.
[9] X. Dai, P. Li, Y. Sui, C. Zhang, Synthesis and performance of flexible epoxy resin with long alkyl side chains via click reaction, J. Polym. Sci. 59 (7) (2021) 627–637, https://doi.org/10.1002/pol.20210044.
[10] D. Marín, P. Gañán, A. Tercjak, C. Castro, D.H. Builes, Phase distribution changes of neat unsaturated polyester resin and their effects on both thermal stability and dynamic-mechanical properties, J. Appl. Polym. Sci. 138 (44) (2021) 51308, https://doi.org/10.1002/app.51308.

[11] W.B. Ying, H.S. Yang, D.S. Moon, Epoxy resins toughened with in situ azide-alkyne polymerized polysulfones, J. Appl. Polym. Sci. 135 (5) (2018) 45790–45802, https://doi.org/10.1002/app.45790.
[12] N.G. Ozdemir, T. Zhang, H. Hadavinia, I. Aspin, F. Scarpa, Glass fibre reinforced polymer composites toughened with acrylonitrile butadiene nanorubber, Compos. Part B-Eng. 88 (2016) 182–188, https://doi.org/10.1016/j.compositesb.2015.09.004.
[13] J. Wang, K. Yu, P. Xiao, L. Li, C. Wang, Z. Wang, D. Guo, Y.K. Kit Richard, Y. Lu, Killing two birds with one stone strategy inspired advanced batteries with superior thermal safety: a comprehensive evaluation, Chem. Eng. J. 515 (2025) 163272, https://doi.org/10.1016/j.cej.2025.163272.
[14] W. Liu, Y. Zhou, J. Wang, Y. Hu, W. Hu, Enhancing low-temperature CO removal in complex flue gases: a study on La and Cu doped Co_3O_4 catalysts under real-world combustion environment, J. Hazard. Mater. 470 (2024) 134174, https://doi.org/10.1016/j.jhazmat.2024.134174.
[15] J. Wang, J. Yang, W. Bai, Z. Wang, K. Yu, Y. Lu, C. Han, Thermal runaway and jet flame features of LIBs undergone high-rate charge/discharge: an investigation, J. Energy Chem. 103 (2025) 826–837, https://doi.org/10.1016/j.jechem.2024.12.004.
[16] Y. Xu, J. Long, R. Zhang, Y. Du, S. Guan, Y. Wang, L. Huang, H. Wei, L. Liu, Y. Huang, Greatly improving thermal stability of silicone resins by modification with POSS, Polym. Degrad. Stabil. 174 (2020) 109082, https://doi.org/10.1016/j.polymdegradstab.2020.109082.
[17] H. Hou, J. Li, X. Li, J. Forth, J. Yin, X. Jiang, B.A. Helms, T.P. Russell, Interfacial activity of amine-functionalized polyhedral oligomeric silsesquioxanes (POSS): a simple strategy to structure liquids, Angew. Chem. Int. Ed. 58 (30) (2019) 10142–10147, https://doi.org/10.1002/anie.201903420.
[18] M. Mohammadi, H. Fazli, M. Karevan, J. Davoodi, The glass transition temperature of PMMA: a molecular dynamics study and comparison of various determination methods, Eur. Polym. J. 91 (2017) 121–133, https://doi.org/10.1016/j.eurpolymj.2017.03.056.
[19] W.-C. Yang, S.-H. Wu, Y.-F. Chen, A. Nelson, C.-M. Wu, Y.-S. Sun, Effects of the density of chemical cross-links and physical entanglements of ultraviolet-irradiated polystyrene chains on domain orientation and spatial order of polystyrene-block-poly(methyl methacrylate) nano-domains, Langmuir 35 (43) (2019) 14017–14030, https://doi.org/10.1021/acs.langmuir.9b02054.
[20] S.-W. Kuo, F.-C. Chang, POSS related polymer nanocomposites, Prog. Polym. Sci. 36 (12) (2011) 1649–1696, https://doi.org/10.1016/j.progpolymsci.2011.05.002.
[21] H.L. Liu, Y.F. Chen, M.Z. Chai, Y.Q. Wu, K.L. Xue, L. Liu, Y.D. Huang, High-performance carbon fiber-reinforced epoxy resin composites based on novel, environmentally friendly, stability, and heat-moisture resistant nano emulsion encapsulated POSS sizing agent interface modification, Compos. Part B-Eng. 284 (2024) 111697, https://doi.org/10.1016/j.compositesb.2024.111697.
[22] C. Liu, D.Y. Zhuang, Y. Zhou, J.H. Liao, S.P. Dai, C.W. Pan, Y.T. Li, L.Z. Dai, W. Wang, Mechanically reinforced and flame-retardant epoxy resin nanocomposite based on molecular engineering of POSS, Polym. Test. 143 (2025) 108719, https://doi.org/10.1016/j.polymertesting.2025.108719.
[23] A. Fina, D. Tabuani, A. Frache, G. Camino, Polypropylene–polyhedral oligomeric silsesquioxanes (POSS) nanocomposites, Polymer 46 (19) (2005) 7855–7866, https://doi.org/10.1016/j.polymer.2005.06.121.
[24] J. Yang, Y. Zhang, M. Hao, J. Zhi, X. Qian, Synergistically toughened epoxy resin based on modified-POSS triggered interpenetrating network, Polymer 268 (2023) 125719, https://doi.org/10.1016/j.polymer.2023.125719.
[25] M. Hao, J. Yang, C. Zhu, Y. Zhang, X. Qian, J. Zhi, L. Liu, Y. Huang, Construction of “Octopus"-like POSS nanostructure triggerring interpenetrating network for high-performance epoxy thermosets and CFRP composites, Compos. Sci. Technol. 270 (2025) 111273, https://doi.org/10.1016/j.compscitech.2025.111273.
[26] W. Zhang, G. Camino, R. Yang, Polymer/polyhedral oligomeric silsesquioxane (POSS) nanocomposites: an overview of fire retardance, Prog. Polym. Sci. 67 (2017) 77–125, https://doi.org/10.1016/j.progpolymsci.2016.09.011.
[27] L. Yang, X. Liu, B. Song, S. Yang, X. Zhang, C. Zhao, Y. Wu, L. Zhang, Y. Huang, Selective adsorption of silver(I) by dimercaptosuccinic acid (DMSA) functionalized polyhedral oligomeric silsesquioxane (POSS)-based hybrid polymer: behavior and mechanism, React. Funct. Polym. 209 (2025) 106170, https://doi.org/10.1016/j.reactfunctpolym.2025.106170.
[28] K. Mishra, D. Gidley, R.P. Singh, Influence of self-assembled compliant domains on the polymer network and mechanical properties of POSS-epoxy nanocomposites under cryogenic conditions, Eur. Polym. J. 116 (2019) 283–290, https://doi.org/10.1016/j.eurpolymj.2019.02.034.
[29] B. Zhang, X. Li, M. Zeng, J. Cao, COMFO: integrated deep learning model facilitates discovery of multifunctional polyimide materials, Polymer 320 (2025) 128081, https://doi.org/10.1016/j.polymer.2025.128081.
[30] A. Jha, A. Chandrasekaran, C. Kim, R. Ramprasad, Impact of dataset uncertainties on machine learning model predictions: the example of polymer glass transition temperatures, Model. Simulat. Mater. Sci. Eng. 27 (2) (2019) 024002, https://doi.org/10.1088/1361-651X/aaf8ca.
[31] I. Blanco, F.A. Bottino, G. Cicala, A. Latteri, A. Recca, A kinetic study of the thermal and thermal oxidative degradations of new bridged POSS/PS nanocomposites, Polym. Degrad. Stabil. 98 (12) (2013) 2564–2570, https://doi.org/10.1016/j.polymdegradstab.2013.09.017.
[32] C. Li, A. Strachan, Molecular dynamics predictions of thermal and mechanical properties of thermoset polymer EPON862/DETDA, Polymer 52 (13) (2011) 2920–2928, https://doi.org/10.1016/j.polymer.2011.04.041.
[33] B. Kim, J. Choi, S. Yang, S. Yu, M. Cho, Multiscale modeling of interphase in crosslinked epoxy nanocomposites, Compos. Part B-Eng. 120 (2017) 128–142, https://doi.org/10.1016/j.compositesb.2017.03.059.
[34] E. Franchini, J. Galy, J.-F. Gérard, D. Tabuani, A. Medici, Influence of POSS structure on the fire retardant properties of epoxy hybrid networks, Polym. Degrad. Stabil. 94 (10) (2009) 1728–1736, https://doi.org/10.1016/j.polymdegradstab.2009.06.025.
[35] Y. Li, H. Li, C. Song, Z. Zhu, X. Ma, Molecular dynamics simulations of the micro mechanism of functionalized SiO2 nanoparticles and carbon nanotubes modified epoxy resin adhesives, Polym. Compos. 46 (2) (2024) 1587–1603, https://doi.org/10.1002/pc.29059.
[36] P.-H. Lin, R. Khare, Molecular simulation of cross-linked epoxy and Epoxy−POSS nanocomposite, Macromolecules 42 (12) (2009) 4319–4327, https://doi.org/10.1021/ma9004007.
[37] D.Z. Chen, W. Sun, C.X. Qian, L.M. Reyes, A.P.Y. Wong, Y.C. Dong, J. Jia, K. K. Chen, G.A. Ozin, Porous NIR photoluminescent silicon Nanocrystals-POSS composites, Adv. Funct. Mater. 26 (28) (2016) 5102–5110, https://doi.org/10.1002/adfm.201601251.
[38] N. Jouault, P. Vallat, F. Dalmas, S. Said, J. Jestin, F. Boué, Well-Dispersed fractal aggregates as filler in Polymer-silica nanocomposites: long-range effects in rheology, Macromolecules 42 (6) (2009) 2031–2040, https://doi.org/10.1021/ma801908u.
[39] K. Dean, W.D. Cook, P. Burchill, M. Zipper, Curing behaviour of IPNs formed from model VERs and epoxy systems: part II. Imidazole-cured epoxy, Polymer 42 (8) (2001) 3589–3601, https://doi.org/10.1016/S0032-3861(00)00745-X.
[40] Y. Zhang, G. Wang, Y. Xu, J. Sun, X. Zhang, T. Zheng, L. Zhang, POSS/EHTPB synergistically toughened epoxy resin for cryogenic application, Polymer 300 (2024) 127013, https://doi.org/10.1016/j.polymer.2024.127013.
[41] W.L. Tsang, A.C. Taylor, Fracture and toughening mechanisms of silica- and core-shell rubber-toughened epoxy at ambient and low temperature, J. Mater. Sci. 54 (22) (2019) 13938–13958, https://doi.org/10.1007/s10853-019-03893-y.
[42] M.R. Ricciardi, I. Papa, A. Langella, T. Langella, V. Lopresto, V. Antonucci, Mechanical properties of glass fibre composites based on nitrile rubber toughened modified epoxy resin, Compos. Part B-Eng. 139 (2018) 259–267, https://doi.org/10.1016/j.compositesb.2017.11.056.
[43] K.N. Raftopoulos, K. Pielichowski, Segmental dynamics in hybrid polymer/POSS nanomaterials, Prog. Polym. Sci. 52 (2016) 136–187, https://doi.org/10.1016/j.progpolymsci.2015.01.003.
[44] S. Sasidharan, A. Anand, Epoxy-based hybrid structural composites with nanofillers: a review, Ind. Eng. Chem. Res. 59 (28) (2020) 12617–12631, https://doi.org/10.1021/acs.iecr.0c01711.
[45] K.N. Raftopoulos, C. Pandis, L. Apekis, P. Pissis, B. Janowski, K. Pielichowski, J. Jaczewska, Polyurethane–POSS hybrids: molecular dynamics studies, Polymer 51 (3) (2010) 709–718, https://doi.org/10.1016/j.polymer.2009.11.067.
[46] W. Jiao, G. Niu, D. Bai, Y. Zheng, H. Wang, Y. Liu, Interlaminar toughness of carbon fiber/epoxy laminates interleaved by nanofibrous veils: from molecular structure to macroscopic properties, Compos. Sci. Technol. 267 (2025) 111205, https://doi.org/10.1016/j.compscitech.2025.111205.
[47] E. Rouhi, K. Bahrami, M. Poorabdollah, Remarkable enhancement of physical-mechanical properties in unsaturated polyester resin composites using SiO_2@CTBN hybrid particles, Polym. Compos. 46 (12) (2025) 10908–10922, https://doi.org/10.1002/pc.29661.
[48] M. Sharifi, C. Jang, C.F. Abrams, G.R. Palmese, Epoxy polymer networks with improved thermal and mechanical properties via controlled dispersion of reactive toughening agents, Macromolecules 48 (20) (2015) 7495–7502, https://doi.org/10.1021/acs.macromol.5b00677.
[49] J. Choi, S. Yu, S. Yang, M. Cho, The glass transition and thermoelastic behavior of epoxy-based nanocomposites: a molecular dynamics study, Polymer 52 (22) (2011) 5197–5203, https://doi.org/10.1016/j.polymer.2011.09.019.
[50] P. Badrinarayanan, W. Zheng, Q. Li, S.L. Simon, The glass transition temperature versus the fictive temperature, J. Non-Cryst. Solids 353 (26) (2007) 2603–2612, https://doi.org/10.1016/j.jnoncrysol.2007.04.025.
[51] X. Wang, Y.A. Hu, L. Song, W.Y. Xing, H.D. Lu, Thermal degradation behaviors of epoxy resin/POSS hybrids and phosphorus-silicon synergism of flame retardancy, J. Polym. Sci., Part B: Polym. Phys. 48 (6) (2010) 693–705, https://doi.org/10.1002/polb.21939.
[52] T. Miyata, Y.K. Sato, Y. Kawagoe, K. Shirasu, H.-F. Wang, A. Kumagai, S. Kinoshita, M. Mizukami, K. Yoshida, H.-H. Huang, T. Okabe, K. Hagita, T. Mizoguchi, H. Jinnai, Effect of inorganic material surface chemistry on structures and fracture behaviours of epoxy resin, Nat. Commun. 15 (2024) 1898, https://doi.org/10.1038/s41467-024-46138-6.
[53] M. Kumar, M.D. Barbhai, Sustainable fire safety solutions: bioactive natural polysaccharides and secondary metabolites as innovative fire retardants for textiles, Emerg. Manag. Sci. Technol. 3 (2023) 17, https://doi.org/10.48130/EMST-2023-0017.
[54] X. Jiang, Y. Hou, Y. Wang, F. Chu, J. Zhu, L. Song, Y. Hu, W. Hu, Solvation chemistry enables eutectogels with ultrahigh autofluorescence, toughness, and adhesion under extreme environments, Adv. Funct. Mater. 35 (2) (2024) 2412313, https://doi.org/10.1002/adfm.202412313.
[55] J. Wang, W. Liu, Y. Hu, L. Song, Y. Hu, Y. Hou, W. Hu, Optimizing low-temperature CO oxidation under realistic combustion conditions: the impact of CeO_2 morphology on Au/CeO_2 catalysts, J. Hazard. Mater. 487 (2025) 137182, https://doi.org/10.1016/j.jhazmat.2025.137182.
[56] X. Wang, F.L. Gao, H.Y. Zhao, L. Tian, S. Li, S. Wang, Z.Z. Yu, X. Li, Polymer-based dielectric composite films with excellent dielectric energy storage and thermal management capabilities, Adv. Funct. Mater. (2025) 12371, https://doi.org/10.1002/adfm.202512371.
[57] C. Qian, R. Bei, T. Zhu, W. Zheng, S. Liu, Z. Chi, M.P. Aldred, X. Chen, Y. Zhang, J. Xu, Facile strategy for intrinsic Low-k dielectric polymers: molecular design

based on secondary relaxation behavior, Macromolecules 52 (12) (2019) 4601–4609, https://doi.org/10.1021/acs.macromol.9b00136.
[58] Z.Y. Peng, A. Ye, L. Zhang, X.L. Li, C. Lian, C.Z. Li, Micro-crosslinked polyimide nanocomposites with low dielectric constant and low dielectric loss for microwave antenna with molecular dynamics, Compos. Commun. 46 (2024) 101804, https://doi.org/10.1016/j.coco.2023.101804.
[59] W. Zhang, A.H.E. Müller, Architecture, self-assembly and properties of well-defined hybrid polymers based on polyhedral oligomeric silsequioxane (POSS), Prog. Polym. Sci. 38 (8) (2013) 1121–1162, https://doi.org/10.1016/j.progpolymsci.2013.03.002.
[60] F. Chu, Y. Hu, W. Hu, L. Song, Y. Hu, Advancements in monomers and reinforcements of unsaturated polyester composites: traditional, bio-based, and flame-retardant types, Compos. Part B-Eng. 294 (2025) 112171, https://doi.org/10.1016/j.compositesb.2025.112171.